Analysis of the Kinetic Mechanism of Enterococcal NADH Peroxidase Reveals Catalytic Roles for NADH Complexes with both Oxidized and Two-Electron-Reduced Enzyme Forms†

Edward J. Crane, III, Derek Parsonage, Leslie B. Poole, and Al Claiborne*

Department of Biochemistry, Wake Forest University Medical Center, Winston-Salem, North Carolina 27157

Received May 12, 1995; Revised Manuscript Received August 31, 1995®

ABSTRACT: Anaerobic titrations of the two-electron-reduced NADH peroxidase (EH_2) with NADH and 3-acetylpyridine adenine dinucleotide (AcPyADH) yield the respective complexes without significant formation of the four-electron-reduced enzyme (EH_4). Further analysis of the EH_2/EH_4 redox couple, however, yields a midpoint potential of −312 mV for the free enzyme at pH 7. The catalytic mechanism of the peroxidase has been evaluated with a combination of kinetic and spectroscopic approaches, including initial velocity and enzyme-monitored turnover measurements, anaerobic stopped-flow studies of the reactions of both oxidized enzyme (E) and EH_2 with NADH and AcPyADH, and diode-array spectral analyses of both the reduction of E → EH_2 by NADH and the formation of EH_2·NADH. Overall, these results are consistent with rapid formation of an E·NADH complex with distinct spectral properties and a rate-limiting hydride transfer step that yields EH_2, with no direct evidence for intermediate $FADH_2$ formation. The EH_2·NADH complex described previously [Poole, L. B., & Claiborne, A. (1986) *J. Biol. Chem. 261*, 14525−14533] is not catalytically competent and reacts relatively slowly with H_2O_2. Stopped-flow analyses do, however, support the very rapid formation of an EH_2·NADH* intermediate, with spectral properties that distinguish it from the static EH_2·NADH form, and yield a first-order rate constant for the conversion between the two species that is smaller than k_{cat}. The combined rapid-reaction and steady-state data are best accommodated by a limiting type of ternary complex mechanism very similar to that proposed previously [Parsonage, D., Miller, H., Ross, R. P., & Claiborne, A. (1993) *J. Biol. Chem. 268*, 3161−3167].

The flavoprotein disulfide reductase family consists of three distinct enzyme classes represented by glutathione reductase (GR),[1] thioredoxin reductase (TrR), and NADH peroxidase (Npx) (Williams, 1992; Miller et al., 1995). The peroxidase and the homologous NADH oxidase (Nox), as isolated originally from the heme-deficient, Gram-positive organism *Enterococcus faecalis* 10C1 (ATCC 11700; formerly *Streptococcus faecalis*), have been extensively characterized (Claiborne et al., 1993, 1994). Sequence analyses (Ross & Claiborne, 1991, 1992), combined with high-resolution X-ray structures (Stehle et al., 1991, 1993) for the peroxidase and its complex with NADH, have focused on the comparison between the two flavoprotein peroxide reductases and enzymes of the GR class. A major point of contrast concerns the redox-active cysteine-sulfenic acid (Cys-SOH) derivatives of Cys42 which are found in both Npx and Nox and which function (as the reduced Cys42-SH) in concert with the flavin to reduce H_2O_2 and O_2, respectively, to H_2O (Claiborne et al., 1993). All members of the GR and TrR classes utilize redox-active disulfides in catalysis (Williams, 1992). Recent work from this laboratory (Parsonage & Claiborne, 1995) has shown that peroxidase mutants lacking Cys42 have indeed lost the non-flavin redox center and are virtually devoid of activity, and the refined 2.0 Å structures of the C42S and C42A proteins confirm the absence of other unanticipated structural changes (Mande et al., 1995). In comparing the active-site structures of the peroxidase and GR, we have also shown that, while the Npx L40C mutant does form a disulfide with Cys42, localized structural changes induced on formation of the S−S bridge eliminate its ability to assist in redox catalysis with the flavin (Miller et al., 1995).

While several members of the disulfide reductase family play important roles in cellular defenses against oxidative stress (Claiborne et al., 1992), only the enterococcal peroxidase and mercuric reductase [Hg(II) → Hg^0; Walsh et al., 1988] catalyze the direct reductions of potentially toxic substrates. Though clearly an enzyme of the GR class, mercuric reductase is atypical in that it does not reduce a disulfide substrate, it has an auxiliary C-terminal disulfide which must also be reduced, and it cycles in turnover between EH_2 and EH_2·NADPH forms (Williams, 1992). Miller et al. (1986) demonstrated that the EH_2 form, although it binds Hg(II) tightly, does not transfer electrons to the substrate. An initial priming reaction converts E → EH_2,

† This work was supported by National Institutes of Health Grant GM-35394. E.J.C. is the recipient of National Research Service Award GM-16274.

* To whom correspondence should be addressed at Department of Biochemistry, Wake Forest University Medical Center, Medical Center Boulevard, Winston-Salem, NC 27157. Telephone: (910) 716-3914.

® Abstract published in *Advance ACS Abstracts,* October 15, 1995.

[1] Abbreviations: GR, glutathione reductase; TrR, thioredoxin reductase; Npx, NADH peroxidase; Nox, NADH oxidase; Cys-SOH, cysteine-sulfenic acid; E, oxidized enzyme; EH_2, two-electron-reduced enzyme; EH_4, four-electron-reduced enzyme; E(Cys42-SO_3H), peroxide-inactivated peroxidase containing sulfonic acid derivative of Cys42; AcPyADH, 3-acetylpyridine adenine dinucleotide (reduced); $E'°$, midpoint redox potential at pH 7.0; E_h, calculated system redox potential; E_1, midpoint potential for the redox couple EH_2/EH_4; E_2, midpoint potential for the redox couple E/EH_2.

0006-2960/95/0434-14114$09.00/0

and 2 equiv of NADPH are required to effect reduction of the first Hg(II) → Hg^0. These features of the mercuric reductase mechanism offer a sharp contrast to the classical ping-pong kinetic schemes for the other enzymes of the GR class, which cycle between E and EH_2 states in catalysis.

Similarly, previous work from this laboratory (Parsonage et al., 1993), based on a steady-state analysis of the recombinant NADH peroxidase, led to the proposal of a limiting type of ternary complex mechanism for the enzyme, involving a central EH_2·NADH species. Stoll and Blanchard (1988), on the basis of studies with the commercially-available NADH peroxidase from *E. hirae* (ATCC 8043; formerly *S. faecalis*), also suggested a catalytic role for the EH_2·NADH complex, with an initial E → EH_2 priming reaction similar to that demonstrated for mercuric reductase. The classical ping-pong kinetic patterns observed with the peroxidase were attributed in part to the tight binding measured in static titrations for EH_2·NADH (Parsonage et al., 1993). In order to provide a more detailed analysis of the proposed mechanism, we present here the results of steady-state and rapid-reaction experiments designed to test the catalytic competency of the peroxidase EH_2·NADH complex.

EXPERIMENTAL PROCEDURES

Materials. NAD^+, NADH, and NADPH were purchased from Boehringer Mannheim, hydrogen peroxide (30%) was from Mallinckrodt, and D-[1-^{2}H]glucose (97 atom % ^{2}H), glucose dehydrogenase from *Bacillus megaterium*, AcPy-ADH, protocatechuate dioxygenase, and protocatechuic acid were from Sigma. All other chemicals, as purchased from sources previously described (Parsonage & Claiborne, 1995), were of the best grades available. Recombinant NADH peroxidase was expressed and purified as described by Parsonage et al. (1993), and the peroxide-inactivated enzyme [E(Cys42-SO_3H)] was prepared by the method of Poole and Claiborne (1989a), with 1 mM azide present to inhibit catalase. NADH peroxidase concentration is expressed as the concentration of enzyme-bound flavin, as determined by absorbance at 450 nm [ϵ_{450} = 10 900 M^{-1} cm^{-1} for native, oxidized enzyme (Poole & Claiborne, 1986)]. Solution pH was determined using an Orion SA 720 pH meter with a Ross combination electrode which had been calibrated between pH 7.00 and either 4.00 or 10.00 at room temperature (7.11 and either 3.99 or 10.27 at 5 °C).

Synthesis of NADH. (4*S*)-[4-^{2}H]NADH was prepared using a previously-described procedure (Ottolina et al., 1989), with the following modification: 50 mg of NAD^+ in 3.0 mL of 20 mM triethanolamine base was titrated to pH 7.5 with 2 M KOH. 12.7 mg of either glucose or [1-^{2}H]glucose and 25 units of glucose dehydrogenase were added to initiate reduction. Small aliquots (1−3 μL) of 2 M KOH were added throughout the reaction to keep the pH at ~7.5. Reactions were generally complete (85−90% of theoretical yields) after 2.5−4 h, based on the absence of further changes in both pH and 340 nm absorbance. The solution was then frozen at −70 °C and lyophilized, yielding a hygroscopic yellow powder, which was stored desiccated and protected from light at −20 °C. The NADH was purified (Orr & Blanchard, 1984) in 7−10 mg aliquots on the day of use. All kinetic isotope effects were determined using (4*S*)-[4-^{1}H]NADH and (4*S*)-[4-^{2}H]NADH which had been prepared in parallel by this method.

Steady-State Kinetics. NADH peroxidase activity was routinely measured using the previously-described procedure (Poole & Claiborne, 1986). Steady-state kinetic parameters (k_{cat} and K_m for both H_2O_2 and the reduced pyridine nucleotide substrate) were determined either with an Applied Photophysics DX.17MV stopped-flow spectrophotometer thermostated at 5 °C or with a Gilford 260 recording spectrophotometer thermostated at 25 °C. In the stopped-flow spectrophotometer, a 50−100 nM solution of enzyme (final concentration) in the appropriate buffer (pH 7.0 or 8.5) was mixed with substrates in the same buffer, and the decrease in absorbance at 340 nm due to oxidation of NADH was followed. This technique allowed for the determination of initial velocities at concentrations of NADH as low as 1.5 μM (A_{340} = 0.009), provided measurements were repeated nine times and the average values were taken [K_m(NADH) at 5 °C, pH 7.0 = 3.0 μM].

Static Titrations. Static titrations were performed using either a Hewlett-Packard Model 8451A or 8452A single-beam diode-array spectrophotometer, essentially as described previously (Poole & Claiborne, 1986). All spectra were corrected for dilution due to the volume of titrant added. E'° for the peroxidase EH_2/EH_4 redox couple was determined by NADPH titration in the presence of 1 mM $NADP^+$ (Veine et al., 1994).

Stopped-Flow Kinetics. Stopped-flow kinetics were analyzed using the Applied Photophysics instrument as described previously (Parsonage & Claiborne, 1995). NADH peroxidase was prepared by first titrating the enzyme into the desired form (E or EH_2). The recombinant wild-type peroxidase contains approximately 25% of the air-stable EH_2 form, as purified (Parsonage et al., 1993). For experiments requiring fully oxidized enzyme (E), the purified protein was titrated with H_2O_2 as described previously (Parsonage et al., 1993). The stable EH_2 form of the enzyme was prepared aerobically by titrating E with NADH and monitoring the reduction spectrally. The enzyme resulting from either procedure was then equilibrated into the appropriate buffer, and excess H_2O_2 or NAD^+ was removed by centrifuging three times in a CM-30 microconcentrator (Amicon). All buffers contained 0.1 M potassium acetate (Poole & Claiborne, 1986). Enzyme solutions were prepared in specially-designed glass tonometers in order to allow anaerobiosis by alternating cycles of evacuation and oxygen-free nitrogen, as described earlier (Parsonage & Claiborne, 1995). For experiments with the static EH_2·NADH complex, the air-stable EH_2 form was taken in a tonometer fitted with a side-arm cuvette, and the contents of the tonometer were then made anaerobic. A syringe containing anaerobic NADH was added, and the enzyme was titrated in the tonometer to the EH_2·NADH form. Solutions of substrates in glass syringes were made anaerobic by bubbling with nitrogen for at least 20 min. The stopped-flow system was made anaerobic by using an oxygen-scrubbing solution containing protocatechuate dioxygenase and protocatechuic acid, as described previously (Parsonage & Claiborne, 1995).

Rapid-reaction studies were also carried out in the laboratory of Dr. David P. Ballou at the University of Michigan, using a Hi-Tech SF-61 stopped-flow apparatus equipped with a diode-array detector (Pollegioni et al., 1994).

Data Analysis. Data from the stopped-flow spectrophotometer were analyzed with either (1) the Applied Photophysics DX.17MV analysis software, for performing linear

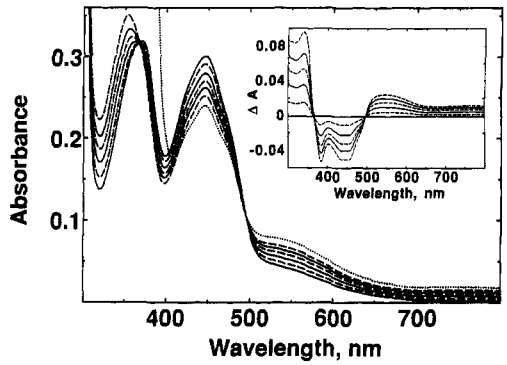

FIGURE 1: Anaerobic NADH titration of Npx EH_2. The cuvette contained 23 nmol of enzyme (FAD), plus an oxygen-scrubbing system consisting of 0.3 μmol of protocatechuic acid and 0.02 unit of protocatechuate dioxygenase, in 0.7 mL of 50 mM potassium phosphate, pH 7.0, plus 0.6 mM EDTA at 23 °C. The EH_2 form was generated by titrating E with 0.91 equiv of NADH/FAD. Spectra shown, in order of decreasing absorbance at 450 nm, represent EH_2 (—) and EH_2 plus 0.15 (- - -), 0.30 (—), 0.45 (- - -), 0.60 (—), 0.76 (- - -), and 22 (•••) equiv of NADH/FAD. The final spectrum was obtained after tipping 21 μL of 22 mM NADH from the cuvette side arm. Inset: Difference spectra corresponding to the first five additions of NADH to EH_2.

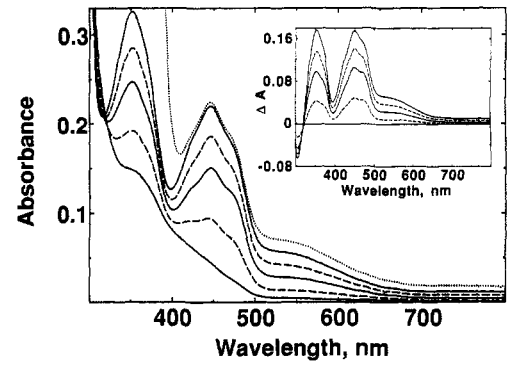

FIGURE 2: Anaerobic NAD^+ titration of Npx EH_4. The cuvette contained 20 nmol of enzyme, plus protocatechuic acid (40 nmol) and protocatechuate dioxygenase (0.02 unit), in 0.7 mL of the pH 7.0 phosphate buffer containing EDTA, at 23 °C. The EH_4 form was generated by titrating E with 1.93 equiv of dithionite/FAD. The dithionite syringe was then exchanged for one containing an anaerobic NAD^+ solution. Spectra shown, in order of increasing absorbance at 450 nm, represent EH_4 (—) and EH_4 plus 0.24 (- - -), 0.48 (—), 0.71 (- - -), and 1.43 (—) equiv of NAD^+/FAD. The final spectrum (•••) was obtained after tipping 21 μL of 22 mM NADH from the cuvette side arm. Inset: Difference spectra corresponding to the NAD^+ titration of EH_4.

regressions or fitting single exponentials to data from individual wavelengths, or (2) their GLOBAL ANALYSIS program for fitting either single or multiple exponentials to data from both single and multiple wavelengths, and for estimating the extinction coefficients of transient enzyme species. In enzyme-monitored turnover experiments, v_0 was determined both from the linear rate of NADH oxidation at 340 nm and as described previously (Gibson et al., 1964). Initial velocity data were analyzed using the ENZFITTER program (Leatherbarrow, 1987) in order to determine both kinetic parameters and the pK_a value for k_{cat}. The KINSIM program (Frieden, 1993) was used to model the pre-steady-state kinetics on a Silicon Graphics Indigo^2 workstation.

RESULTS

EH_2 Complexes with NADH and AcPyADH. As shown in Figure 1, titration of EH_2 with NADH under anaerobic conditions yields the EH_2·NADH complex characterized by increased long-wavelength absorbance extending from 500 to 800 nm. The difference spectra indicate the presence of isosbestic points at 367 and 498 nm, and a plot of ΔA_{750} *versus* added NADH follows the same pattern as seen for titration data at both 540 and 450 nm. The ΔA_{max} at 340 nm confirms the binding of NADH in its reduced form, although the molar ϵ_{340} is decreased and NADH fluorescence is quenched substantially. Recently, we have shown (Parsonage & Claiborne, 1995) that the reduced peroxidase C42S mutant binds NAD^+ (K_d = 20 μM), giving rise to an $FADH_2$ → NAD^+ charge-transfer complex with long-wavelength absorbance (λ_{max} = 740 nm). We therefore provided another experimental test to determine whether the 750 nm absorbance of EH_2·NADH could be attributed to an EH_4·NAD^+ contribution. When the peroxidase EH_4 species is generated by dithionite reduction and titrated anaerobically with NAD^+ (Figure 2), the stoichiometric (with added NAD^+) appearance of EH_2·NADH is observed on each addition of oxidized pyridine nucleotide; in this static experiment, there is no evidence for any stable EH_4·NAD^+ complex with the wild-type peroxidase.

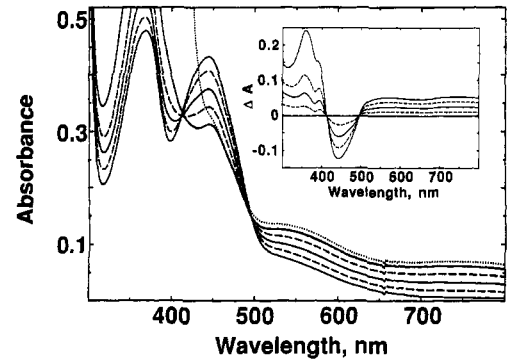

FIGURE 3: Anaerobic AcPyADH titration of Npx EH_2. The cuvette contained 32 nmol of enzyme and the protocatechuate dioxygenase oxygen-scrubbing system in 0.7 mL of pH 7.0 phosphate buffer containing EDTA, at 23 °C. The EH_2 form was generated by titrating E with 0.98 equiv of AcPyADH/FAD. Spectra shown, in order of decreasing absorbance at 450 nm, represent EH_2 (—) and EH_2 plus 0.24 (- - -), 0.49 (—), 0.85 (- - -), 1.34 (—), and 22 (•••) equiv of AcPyADH/FAD. The final spectrum was obtained after tipping 29 μL of 22 mM AcPyADH from the cuvette side arm. Inset: Difference spectra corresponding to the first four additions of AcPyADH to EH_2.

A second preliminary conclusion from this analysis is that the redox potential of the peroxidase EH_2/EH_4 couple is considerably lower than that of NAD^+/NADH ($E'°$ = −320 mV; Loach, 1976). AcPyADH ($E'°$ = −248 mV; Loach, 1976) has been reported to be a good substrate for both the *E. faecalis* (Poole & Claiborne, 1986) and *E. hirae* (Stoll & Blanchard, 1988) NADH peroxidases, and given its higher redox potential, the spectral properties of its EH_2 complex were also examined (Figure 3). Again, there is broad long-wavelength absorbance in the EH_2·AcPyADH complex extending from 500 to 800 nm, and the ΔA_{max} of 360 nm confirms that AcPyADH binds in its reduced form. The $\Delta\epsilon$ at 700 nm (1300 M^{-1} cm^{-1}) is higher than that seen with NADH (~700 M^{-1} cm^{-1}), although the pyridine nucleotide redox potential is 72 mV more positive. These observations further support the conclusion that these EH_2 complexes, and their long-wavelength charge-transfer absorbance bands, do not reflect significant EH_4 contributions. In both cases there

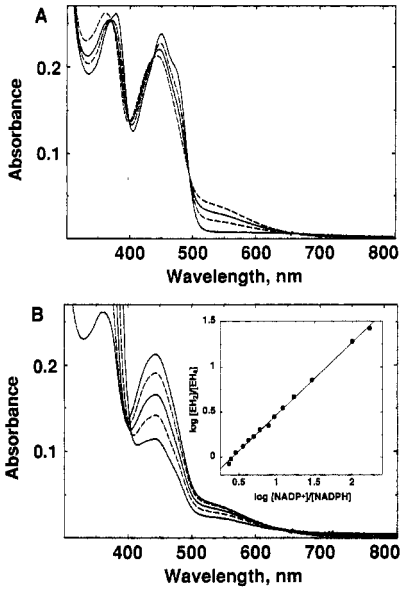

FIGURE 4: Reductive titration of Npx with NADPH in the presence of $NADP^+$. The cuvette contained 15 nmol of enzyme and 0.98 mM $NADP^+$, plus the protocatechuate dioxygenase oxygen-scrubbing system, in 0.7 mL of 50 mM potassium phosphate, pH 7.0, containing 0.1 M potassium acetate and 0.5 mM EDTA, at 23 °C. The enzyme was titrated with an anaerobic 6 mM solution of NADPH. Spectra were recorded after all absorbance changes were complete and have been corrected for dilution. (A) Spectra shown, in order of decreasing absorbance at 450 nm, represent E (—) and E plus 0.33 (- - -), 0.59 (—), and 0.85 (- - -) equiv of NADPH/FAD. (B) Spectra shown, in order of decreasing absorbance at 450 nm, represent EH_2 (—) and EH_2 plus 1.49 (- - -), 4.69 (—), 10 (- - -), and 17.4 (—) equiv of NADPH/FAD. Inset: log of the $[EH_2]/[EH_4]$ ratio (monitored at 450 nm) *versus* log of the $[NADP^+]/[NADPH]$ ratio (monitored at 330 nm). Further details are given in Results.

is enhancement of the 540 nm charge-transfer absorbance attributed to the Cys42-S^- → FAD interaction in EH_2.

Redox Potential of the Peroxidase EH_2/EH_4 Couple. Dithionite titration of the wild-type EH_2 form of the peroxidase yields direct reduction of the flavin with 1.1 equiv of reductant (Poole & Claiborne, 1986); there is no evidence for cooperativity among redox sites in the tetrameric protein. Based on the formation constant for comproportionation of $E + EH_4 \rightleftarrows 2EH_2$, the potential for the EH_2/EH_4 couple must be at least 86 mV lower than that for E → EH_2 reduction (Poole & Claiborne, 1989b). The FAD/$FADH_2$ potentials determined for C42S and C42A mutants in the presence of redox dyes are −219 and −197 mV, respectively; plots of log [E-FAD]/[E-$FADH_2$] *versus* log $[dye_{ox}]/[dye_{red}]$ are linear with a slope of 1, as expected (Parsonage & Claiborne, 1995). Using the nonphysiological substrate NADH, Veine et al. (1994) have determined the E/EH_2 potential for *Escherichia coli* GR, which does not form complexes with NADH or NAD^+ in either redox state. NADPH has been reported to be a poor substrate for NADH peroxidase (Poole & Claiborne, 1986; Stoll & Blanchard, 1988); yet in anaerobic titrations NADPH reduces E → EH_2 relatively rapidly. Furthermore, NADPH reduces EH_2 → EH_4 without any spectral evidence for the formation of either EH_2·NADPH or EH_4·$NADP^+$ complexes analogous to those seen with wild-type and C42S peroxidases, respectively, with NADH and NAD^+. Figure 4 gives the results of NADPH titrations of both E and EH_2 in the presence of 1 mM $NADP^+$. The conversion of E → EH_2 by NADPH under these conditions

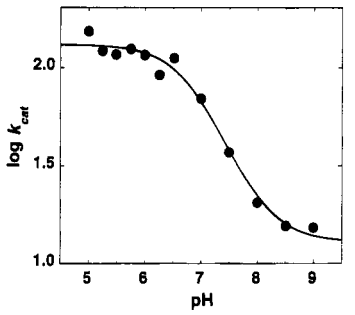

FIGURE 5: pH dependence of k_{cat} with Npx at 25 °C. Initial velocity measurements were made with a Gilford Model 260 recording spectrophotometer thermostated at 25 °C, taking H_2O_2 as the variable substrate at a fixed, saturating [NADH] of 0.16 mM. Enzyme concentration was 0.4−0.7 nM, and the buffers used were 0.1 M potassium acetate (pH 5.0, 5.25), 0.1 M morpholinoethanesulfonic acid (MES)/0.1 M potassium acetate (pH 5.49−6.52), 0.1 M morpholinopropanesulfonic acid (MOPS)/0.1 M potassium acetate (pH 7.0), and 0.1 M *N*-[2-hydroxyethyl]piperazine-*N*′-[2-ethanesulfonic acid] (HEPES)/0.1 M potassium acetate (pH 7.5−9.0). All buffers contained 0.3 mM EDTA. Initial rates at lower pH values were corrected for the spontaneous acid-catalyzed breakdown of NADH. Kinetic parameters were calculated using ENZFITTER.

is stoichiometric with added reductant at each data point, leading to isosbestic behavior at 368 nm [ϵ_{368}(NADPH) = 2650 M^{-1} cm^{-1}; P-L Biochemicals Circular No. OR-18, 1977]. Determination of the E → EH_2 redox potential is precluded in this case, since calculation of the observed potential (E_h) requires a finite value for the ratio $[NADP^+]/[NADPH]$ (Veine et al., 1994). Reduction of EH_2 → EH_4, however, does require excess NADPH; in this measurement [NADPH] is determined directly at 330 nm (isosbestic for EH_2 and EH_4) using ϵ_{330} = 5730 M^{-1} cm^{-1}. The concentrations of EH_2 and EH_4 are measured at 450 nm using ϵ_{450} = 9660 M^{-1} cm^{-1} for EH_2 and $\Delta\epsilon_{450}$ = 8300 M^{-1} cm^{-1} for its reduction to EH_4 (Poole & Claiborne, 1986). As shown in Figure 4, the plot of log $[EH_2]/[EH_4]$ *versus* log $[NADP^+]/[NADPH]$ is linear (slope = 0.8), and E_1 = −312 mV for the EH_2/EH_4 couple. It follows that E_2, the redox potential for E → EH_2, is ≥−226 mV. Since E'° for free NAD^+/NADH is −320 mV, these results indicate clearly that the relative potentials for FAD and NADH in the EH_2·NADH complex are much more effectively separated than the free solution potentials would suggest. This effect is specific for the reduced pyridine nucleotide, however, since titrations of EH_2 with NAD^+, at concentrations well above the reported K_i (Parsonage et al., 1993; Stoll & Blanchard, 1988), do not lead to any spectrally observable changes.

pH Profiles for k_{cat} and $k_{cat}/K_m(H_2O_2)$. We have previously determined steady-state kinetic parameters for the *E. faecalis* peroxidase with NADH at pH 5.5 and 7.5 (Parsonage et al., 1993). Figure 5 gives the pH dependence for k_{cat} at 25 °C. The k_{cat} profile indicates that activity is maximal over the pH range 5.0−6.5, with no apparent limiting ionizations within the E·S complex. k_{cat} decreases over the pH range 6.5−8.5 (slope = −0.53), consistent with a requirement for a protonated species within the enzyme−substrate complex with a pK_a of 6.9 ± 0.2. However, the limiting value of k_{cat} above this pK_a is still 10% (12.8 s^{-1} *versus* 130.5 s^{-1}) of that at pH 5, indicating that the deprotonated form also has significant activity. K_m(NADH) only decreases from 6.3 μM to 4 μM over the pH range 5.5−7.5, while $K_m(H_2O_2)$ decreases more than 10-fold (130 μM to 10.1 μM; Parsonage

Table 1: Steady-State Kinetic Parameters for NADH Peroxidase

	substrates			
	NADH	H_2O_2	AcPyADH	H_2O_2
kinetic parameter, pH 7.0[a]				
K_m	3.0 μM	14.1 μM	2.7 μM	ND[b]
k_{cat}	23.3 s^{-1}		8.5 s^{-1}	
kinetic parameter, pH 8.5[c]				
K_m	0.8 μM	1.1 μM	ND	ND
k_{cat}	3.9 s^{-1}		1.5 s^{-1}	

[a] Initial velocity measurements were made in 50 mM potassium phosphate, 0.1 M potassium acetate, pH 7.0, plus 0.5 mM EDTA, at 5 °C. [b] ND, not determined. [c] Initial velocity measurements were made in 50 mM *N*-[2-hydroxyethyl]piperazine-*N'*-[2-ethanesulfonic acid] (HEPES), 0.1 M potassium acetate, pH 8.5, plus 0.5 mM EDTA, at 5 °C.

et al., 1993). The $k_{cat}/K_m(H_2O_2)$ profile (data not shown) increases linearly over the pH range 5−7.5 (slope = 0.52), indicating a requirement for a deprotonated, reduced enzyme species (pK_a ~7.5) for optimal reaction with H_2O_2. At pH 9, $k_{cat}/K_m(H_2O_2)$ reaches a plateau corresponding to a maximal value of 4.2 × 10^6 M^{-1} s^{-1} at 25 °C, which represents a minimal estimate of the second-order rate constant for the reaction between reduced enzyme and H_2O_2. Relative to the pK_a values of 6.9 ± 0.2 and ~7.5 determined above, we have shown that $pK_a \leq 4.5$ for the catalytic Cys42-SH of EH_2 (Poole & Claiborne, 1986).

Initial Velocity Studies and Primary Deuterium Kinetic Isotope Effect. Initial velocity studies were carried out at 5 °C with both NADH and AcPyADH in order to allow direct comparisons with kinetic parameters from rapid-reaction experiments, and the steady-state values are summarized in Table 1 for both pH 7.0 and 8.5. These data were collected in the stopped-flow spectrophotometer by monitoring ΔA_{340} or ΔA_{363} (NADH or AcPyADH, respectively) at final enzyme concentrations of 50−100 nM. As can be seen with NADH at pH 7.0, only k_{cat}, which is 3-fold lower at 5 °C *versus* 25 °C, is affected significantly by the change in temperature. Given the steady-state parameters for NADH at pH 7.0, 5 °C, we next determined the primary deuterium kinetic isotope effect using synthetic (4*S*)-[4-^{1}H]- and (4*S*)-[4-^{2}H]NADH at fixed, saturating concentrations of NADH (0.18−0.21 mM) and H_2O_2 (2 mM). Initial rates were again measured at 340 nm in the stopped-flow spectrophotometer, but at a final enzyme concentration of 21 μM, in order to allow direct comparison with results from enzyme-monitored turnover. With synthetic (4*S*)-[4-^{1}H]NADH, k_{cat} = 18.2 s^{-1}, comparing favorably with the value of 23.3 s^{-1} presented in Table 1. With (4*S*)-[4-^{2}H]NADH, k_{cat} = 7.7 s^{-1}, giving a value for V_H/V_D = 2.4 and indicating that hydride transfer from NADH is at least partially rate-limiting in turnover.

Enzyme-Monitored Turnover Analyses. As shown in Figure 1, the spectral differences between the peroxidase EH_2 and EH_2·NADH forms are significant. Since we have previously proposed a central catalytic role for EH_2·NADH (Parsonage et al., 1993), and since hydride transfer from NADH is at least partially rate-limiting in turnover, we analyzed the spectral properties of the peroxidase under steady-state conditions. Following the enzyme-monitored turnover method originally described by Gibson et al. (1964), we analyzed the reaction of 21 μM oxidized enzyme in the presence of 0.18 mM NADH and 2 mM H_2O_2, at wavelengths of 450, 568, and 660 nm (Figure 6). At 450 nm

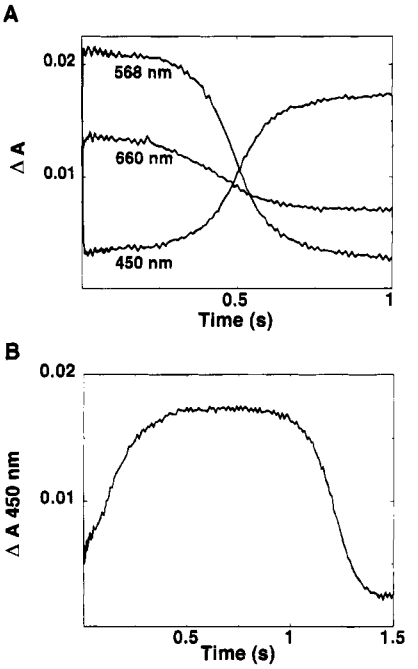

FIGURE 6: Enzyme-monitored turnover of Npx. (A) Enzyme (21 μM, after mixing) was reacted anaerobically with 0.18 mM NADH and 2 mM H_2O_2 in 50 mM phosphate, pH 7.0, containing 0.1 M potassium acetate and 0.6 mM EDTA, at 5 °C, in the Applied Photophysics stopped-flow spectrophotometer. The reaction was monitored by following enzyme absorbance at 450, 568, and 660 nm and NADH absorbance at 340 nm (not shown). (B) EH_2·NADH (12.2 μM), generated anaerobically in the tonometer by NADH titration of E, was mixed with 0.35 mM NADH and 0.25 mM H_2O_2 under otherwise identical conditions. The enzyme absorbance was monitored at 450 nm.

there is a rapid, partial reduction in oxidized enzyme absorbance (complete within 10 ms) followed by a phase corresponding to steady-state turnover. As NADH is exhausted, there is a gradual increase in A_{450} as the enzyme returns to the oxidized state. The initial rapid decrease in absorbance as the enzyme approaches steady state gives a pseudo-first-order rate constant of 516 s^{-1} for the conversion of E to $E_{steady\text{-}state}$ (Gutfreund, 1972), and the turnover number calculated by the method of Gibson et al. (1964) in the steady-state phase is 19.1 s^{-1}, agreeing reasonably well with the k_{cat} value of 23.3 s^{-1} (Table 1). The approach to steady state corresponds to absorbance increases at both 568 and 660 nm. While both EH_2 and EH_2·NADH forms have extinction coefficients at 450 and 568 nm that are lower and higher, respectively, than that of E, only EH_2·NADH has an increased ϵ_{660} (Figures 1 and 4). The results of this analysis are therefore qualitatively consistent with the accumulation of EH_2·NADH during steady-state turnover. Another experimental test of this possibility involves enzyme-monitored turnover analysis of the EH_2·NADH complex, as generated in static titrations such as that shown in Figure 1. Since a spectrally similar species appears to predominate in turnover, there should be very little absorbance change in the approach to steady state. However, as also indicated in Figure 6, there are two surprising observations with this experiment. At 450 nm there is a significant increase in absorbance during the transition from EH_2·NADH → $E_{steady\text{-}state}$, indicating that $E_{steady\text{-}state}$ has an ϵ_{450} more like that of E. Also, the rate of approach to this steady state is very slow (4−5 s^{-1} *versus* 516 s^{-1} for E), further suggesting that the EH_2·NADH complex is not catalytically competent. From the steady-

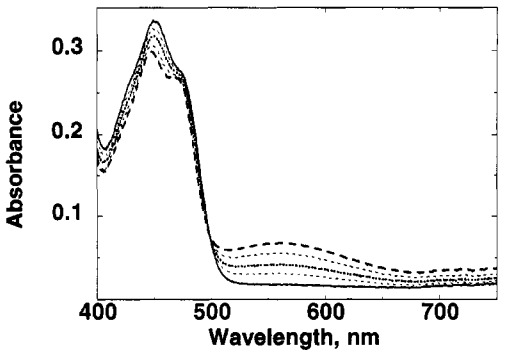

FIGURE 7: Absorption spectra of Npx during turnover. EH_2 (30.2 μM) was mixed, under anaerobic conditions, with 0.34 mM NADH and 2 mM H_2O_2 in the standard pH 7.0 phosphate/acetate buffer at 4 °C, using the Hi-Tech SF-61 stopped-flow spectrophotometer equipped with a diode-array detector. Spectra shown, in order of decreasing absorbance at 550 nm, represent $E_{steady\text{-}state}$ (— —; 0.101 s), enzyme at 0.476 s (- - -), 0.526 s (•••), and 0.576 s (- - -), and E_{ox} (—; 1.501 s).

state phase that does eventually appear, k_{cat} = 18.6 s^{-1}, in excellent agreement with the turnover number determined with E. This indicates that nothing irreversible has affected the intrinsic catalytic activity of the enzyme, once the slow approach to steady state is overcome. In a parallel experiment with EH_2 generated in a static titration, the rate of approach to steady state is similar (480 s^{-1}) to that seen with E; simple reduction to EH_2 has no effect on the catalytic competency of the enzyme. Furthermore, since we have provided considerable evidence that EH_2·NADH does not include any significant EH_4 contribution, flavin reduction is not the basis for the behavior of EH_2·NADH in these experiments.

Diode-Array Analysis. In order to provide a full characterization of the spectral properties of the enzyme during steady-state turnover, enzyme-monitored turnover experiments mixing 30.2 μM EH_2 (final concentration) with 10 equiv of NADH and 2 mM H_2O_2 were performed, using a stopped-flow spectrophotometer equipped with a diode-array detector (Pollegioni et al., 1994). We are indebted to Dr. David P. Ballou, University of Michigan, for his assistance with this analysis. As shown in Figure 7, the spectrum of $E_{steady\text{-}state}$ is consistent with the wavelength dependence for the absorbance changes shown for the approach to steady state from E in Figure 6. The absorbance at 450 nm for $E_{steady\text{-}state}$ is considerably higher than that for EH_2·NADH (Figure 1), further confirming the observations presented in Figure 6. The spectra shown in Figure 7 correspond to the conversion of $E_{steady\text{-}state}$ → E as NADH is exhausted, and the isosbestic point at 498 nm is identical to that seen in the conversion of EH_2 → EH_2·NADH. In contrast to EH_2 and EH_2·NADH, $E_{steady\text{-}state}$ displays a distinct long-wavelength maximum at 560 nm as well as a resolved shoulder at 468 nm. Very similar spectral properties are seen in the NADH complex of E(Cys42-SO_3H), with isosbestic points in the NADH titration at 372 and 498 nm (Poole & Claiborne, 1989a). This complex also exhibits a relatively high ϵ_{450} with the resolved shoulder at 472 nm and a defined long-wavelength absorbance maximum at 546 nm, with absorbance extending beyond 800 nm. While these comparisons strongly suggest that the species represented by $E_{steady\text{-}state}$ is the E·NADH complex, further analyses of the reduction of E → EH_2 were performed to test this possibility.

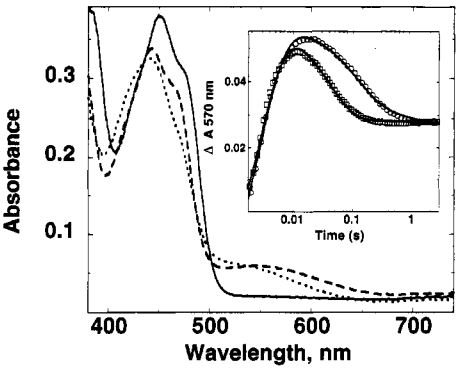

FIGURE 8: Stopped-flow analysis of the NADH reduction of Npx E → EH_2. Diode-array spectra were measured with the Hi-Tech instrument on mixing 34.2 μM E (final concentration) with an equimolar concentration of NADH at pH 7.0, 4 °C, under anaerobic conditions. Spectra shown represent E (—), enzyme at 11 ms (- - -), and EH_2 (•••; 238 ms). Inset: Time course for NADH reduction of E → EH_2 and deuterium isotope effect. 79 μM E was mixed anaerobically with 55 μM (4*S*)-[4-^{1}H]NADH (□) or (4*S*)-[4-^{2}H]NADH (○), in the Applied Photophysics stopped-flow instrument, at pH 7.0, 5 °C. The course of reaction was monitored at 570 nm.

Reduction of E → EH_2. Figure 8 gives a diode-array spectral analysis of the anaerobic reduction of E → EH_2, with 34.2 μM enzyme (final concentration) and 1 equiv of NADH. Under these conditions EH_2·NADH formation is precluded, and the kinetic analysis is simplified. The spectral course of reduction involves rapid formation of an intermediate characterized by oxidized flavin absorbance with a resolved shoulder at 470 nm and increased long-wavelength absorbance (λ_{max} ~550 nm) extending from 500 to 740 nm. This species decays to EH_2 in a process which yields isosbestic points at 433, 488, and 523 nm. In order to investigate the kinetics of reduction in more detail and to identify the step involving hydride transfer from NADH, stopped-flow analyses were carried out at 570 nm with 79 μM E (final concentration) and 0.7 equiv of synthetic (4*S*)-[4-^{1}H]- or (4*S*)-[4-^{2}H]NADH, and these kinetic data are also shown in Figure 8. In both cases there is a rapid increase in absorbance followed by a slower decrease in A_{570} which is sensitive to [4-^{2}H]NADH. k_{obs} for this second phase is 25.4 s^{-1} with [4-^{1}H]NADH and 8.6 s^{-1} with the deuterated substrate. The corresponding isotope effects (k_H/k_D) for each of the two phases at 570 nm are 1.03 and 2.95, respectively. Final absorbance spectra taken in each case confirm that EH_2 has been formed. The isotope effect of 2.95 observed in the second phase is comparable to the isotope effect of 2.4 measured on turnover in the presence of saturating substrates and furthermore identifies this step as involving hydride transfer from NADH. The spectral properties of $E_{steady\text{-}state}$ are very similar to those of the intermediate which forms rapidly in the reduction of E, and we conclude that this species is the E·NADH complex.

The observation of similar isotope effects on turnover and on the conversion of E·NADH → EH_2 suggests that EH_2 formation is largely rate-limiting in turnover as well, consistent with the predominant E·NADH spectral contribution in $E_{steady\text{-}state}$. The rate constant of 25.4 s^{-1} observed for EH_2 formation from E·NADH in this experiment compares favorably with the k_{cat} value of 23.3 s^{-1} from the initial velocity data (Table 1). Similar kinetic behavior was observed for NADH reduction of E → EH_2 at pH 8.5 (k_{cat} = 3.9 s^{-1}). At 18.2 μM enzyme and 0.7 equiv of NADH, k_{NADH}

= 88.9 s^{-1} (pseudo-first-order rate constant for E·NADH formation) and k_{red} = 5.6 s^{-1} (first-order rate constant for EH_2 formation from E·NADH). k_{red} decreases 5-fold over the pH range 7.0−8.5 at 5 °C and mirrors the k_{cat} profile given in Figure 5. These results suggest that conversion of E·NADH → EH_2 is largely rate-limiting over the pH range given.

Similar behavior was observed both in steady-state analyses and in stopped-flow measurements of EH_2 formation with AcPyADH. k_{cat} = 8.5 s^{-1} and 1.5 s^{-1} at pH 7.0 and 8.5, respectively (Table 1), and reduction of E → EH_2 with 16 μM enzyme and 0.8 equiv of AcPyADH gives $k_{AcPyADH}$ = 57.2 s^{-1} and k_{red} = 7.0 s^{-1} at pH 7.0. The fast phase observed with 0.7 equiv of AcPyADH corresponds to an increase in A_{660}, as expected for formation of E·AcPyADH. At 450 nm, AcPyADH, unlike NADH, gives clearly biphasic behavior in the reduction of E → EH_2. Further analysis shows that this difference in reduction kinetics with the two substrates is due to the lower ϵ_{450} value for E·AcPyADH (ϵ_{450} = 7950 M^{-1} cm^{-1}), compared with that for E·NADH (ϵ_{450} = 9890 M^{-1} cm^{-1}). As with NADH, comparison of the k_{red} values at pH 7.0 and 8.5 with the respective k_{cat} parameters (Table 1) suggests that conversion of E·AcPyADH → EH_2 is also largely rate-limiting in turnover with AcPyADH. There is no indication that frank flavin reduction and reoxidation account for the biphasic behavior observed with AcPyADH, and the spectral properties of the NADH and AcPyADH complexes of E(Cys42-SO_3H) reflect the difference in ϵ_{450} values observed for E·NADH and E·AcPyADH.

Kinetic Analysis of EH_2·NADH Formation. Diode-array analysis of the formation of EH_2·NADH from E with 5 equiv of NADH (final [NADH] = 0.125 mM) offers excellent kinetic resolution of the E·NADH intermediate and provides indirect evidence suggesting that the release of NAD^+ from EH_2 is rapid, relative to EH_2 formation from E·NADH. When monitored in an independent stopped-flow experiment at 568 nm, the conversion of E → EH_2·NADH exhibits a biphasic increase in absorbance, followed by a slower decrease at 12.6 s^{-1}. The fast phase yields k_{NADH} = 724 s^{-1}, corresponding to a second-order rate constant of 5.8 × 10^6 M^{-1} s^{-1}, and the second rate constant of 28.4 s^{-1}, which is independent of [NADH], matches that for the formation of EH_2 from E·NADH (k_{red} = 25.4 s^{-1}; Figure 8) very well. The increase in A_{568} at these rates is attributed to the following scheme:

$$E + NADH \xrightarrow{5.8 \times 10^6\ M^{-1}\ s^{-1}} E{\cdot}NADH \xrightarrow{28.4\ s^{-1}} EH_2{\cdot}NAD^+$$

$$EH_2{\cdot}NAD^+ \xrightarrow{k_{NAD^+}} EH_2 + NAD^+$$

where $k_{NAD^+} \gg 29$ s^{-1}, and EH_2 rapidly binds NADH to form EH_2·NADH. Simulations of this scheme indicate that values for k_{NAD^+} of 50−150 s^{-1} introduce significant lags between the formation of E·NADH and the formation of EH_2·NADH and require a minimal value of 250 s^{-1} for the NAD^+ off-rate. Diode-array analyses were then performed for the reaction of EH_2 with NADH. The stability of EH_2 under aerobic conditions allowed the removal of NAD^+ by ultrafiltration prior to these experiments. Figure 9 gives the spectral course for the rapid reaction of EH_2 (30.2 μM) with 5 equiv of NADH. At 8.7 ms after mixing a new species has appeared which shares an apparent isosbestic point with EH_2 at 493 nm, with decreased absorbance over the wavelength range 390−490 nm and increased long-wavelength absorbance extending from 500 to 650 nm. This intermediate then decays to a final spectrum characteristic of the EH_2·NADH complex observed in static titrations (Figure 1). Independent stopped-flow analysis at 570 nm, with 88 μM EH_2 and 5 equiv of NADH (Figure 9), gives k_{obs} values of 848 s^{-1} for the rapid increase in absorbance and 10.4 s^{-1} for the slower second phase. The fast phase is attributed to the binding of NADH to EH_2, yielding an EH_2·NADH* complex with spectral properties quite distinct from those of both EH_2 and EH_2·NADH. The slower rate constant of 10.4 s^{-1} compares favorably with that of 12.6 s^{-1} measured for the slow phase in the conversion of E → EH_2·NADH and is not likely to be catalytically significant, since k_{cat} = 23.3 s^{-1}. Inspection of the end-point absorbance spectrum taken in the stopped-flow spectrophotometer confirms the formation of an EH_2·NADH complex indistinguishable from that formed in static titrations, and the extensive characterization of EH_2·NADH in Figures 1 and 2 indicates that there is no significant EH_4·NAD^+ spectral component.

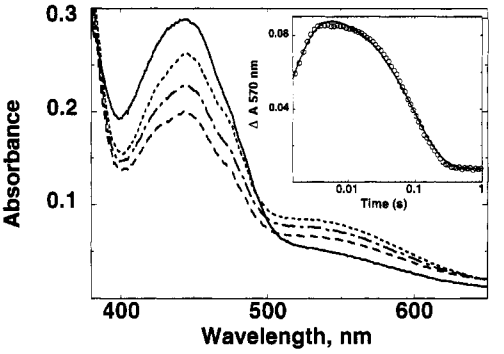

FIGURE 9: Stopped-flow analysis of the reaction of NADH with Npx EH_2. Diode-array spectra were measured with the Hi-Tech instrument on mixing 30.2 μM EH_2 with 0.15 mM NADH under anaerobic conditions at pH 7.0, 4 °C. Spectra shown represent EH_2 (—), enzyme at 9 ms (- - -) and 78 ms (—·—), and EH_2·NADH (— —; 229 ms). Inset: Time course for the reaction of EH_2 with NADH. 88 μM EH_2 was mixed with 0.44 mM NADH at pH 7.0, 5 °C, in the Applied Photophysics stopped-flow under anaerobic conditions. The course of reaction was monitored at 570 nm.

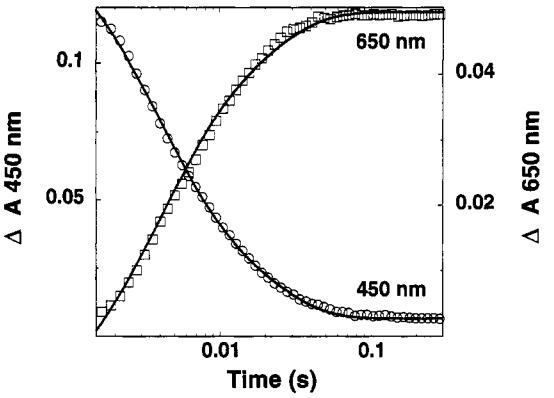

FIGURE 10: Time course for the reaction of AcPyADH with Npx EH_2. 42.2 μM EH_2 was mixed anaerobically with 0.13 mM AcPyADH at pH 7.0, 5 °C, in the Applied Photophysics stopped-flow spectrophotometer. The course of the reaction was monitored at 450 nm (○) and at 650 nm (□).

The Reaction of EH_2 with AcPyADH. Figure 10 gives the kinetic traces observed at 450 and 650 nm on reacting 42.2 μM EH_2 (final concentration) with 3 equiv of AcPyADH. In both cases, there are two phases to the reaction corre-

sponding to k_{obs} values of 281 s^{-1} and 59 s^{-1}. Unlike the conversion of $EH_2 \rightarrow EH_2$·NADH, both observed rates are significantly faster than turnover with AcPyADH (k_{cat} = 8.5 s^{-1}) and are therefore catalytically competent. Although diode-array spectral analyses of this reaction were not carried out, kinetic data collected over the wavelength range 500–650 nm, at 20–30 nm intervals, show that the second phase is characterized by an isosbestic point at ~570 nm. We attribute the faster, pyridine nucleotide-dependent phase to the formation of an EH_2·AcPyADH* complex analogous to EH_2·NADH*. The process corresponding to the second phase has not been identified but may involve the interconversion of, for example, two conformationally distinct forms, giving rise to the EH_2·AcPyADH complex observed in static titrations. This species is characterized by an absorbance spectrum with extinction coefficients higher than those for EH_2·AcPyADH* at wavelengths ≥590 nm. The end-point spectra from stopped-flow experiments at four different concentrations of AcPyADH were identical, again supporting the general conclusion that significant over-reduction to EH_4 does not occur in either the EH_2·AcPyADH or EH_2·NADH complexes.

The Reaction of EH_2 with H_2O_2. We have demonstrated that the static EH_2·NADH complex exhibits a very slow approach to steady state, and this behavior has been confirmed in sequential stopped-flow studies in which EH_2 is first mixed anaerobically with NADH, prior to mixing with excess NADH and H_2O_2 in an enzyme-monitored turnover analysis. The relative concentrations of EH_2, EH_2·NADH*, and EH_2·NADH are determined by the aging time selected before mixing with excess NADH and H_2O_2. With a short aging time of 13 ms, there is only a small fraction of the enzyme which exhibits a slow approach to steady state (monitored at 450 nm). With an aging time of 1 s, however, this slow component is increased 7-fold and accounts for ~75% of the entire ΔA_{450}. A likely explanation for the anomalous approach to steady state observed with EH_2·NADH involves its slow reaction with H_2O_2. When 12 μM EH_2·NADH was reacted with a 20-fold excess of H_2O_2, the k_{obs} value for the monophasic increase in A_{450} was only 14.6 s^{-1}, which is slower than the k_{cat} value of 23.3 s^{-1}. In summary, the EH_2·NADH complex is not catalytically competent because its rate of formation from EH_2·NADH* (10.4 s^{-1}), its rate of reaction with H_2O_2 (14.6 s^{-1}), and its rate of approach to steady state (4–5 s^{-1}) are all slower than k_{cat}. In contrast, the rate of formation of EH_2·AcPyADH from EH_2·AcPyADH* (59 s^{-1}) is considerably faster than the respective turnover number, and sequential stopped-flow experiments similar to that described above, but with AcPyADH replacing NADH, give no indication of any slow component in the approach to steady state at increasing aging times.

Since EH_2·NADH* cannot be prepared by static titration methods, the direct reaction of EH_2 with H_2O_2 was investigated. Figure 11 gives kinetic traces at both 450 and 530 nm for the reaction of 17.5 μM EH_2 (final concentration) with 4 equiv of H_2O_2. The k_{obs} value determined from these monophasic processes is 175 s^{-1} at pH 7.0, 5 °C. When k_{obs} was measured at a series of H_2O_2 concentrations under pseudo-first-order conditions, the irreversible second-order dependency also shown in Figure 11 resulted. The second-order rate constant for the reaction of EH_2 with H_2O_2 is 3.0 × 10^6 M^{-1} s^{-1} under these conditions. This value can be compared to that for $k_{cat}/K_m(H_2O_2)$ = 1.7 × 10^6 M^{-1} s^{-1} determined at pH 7.0, 5 °C.

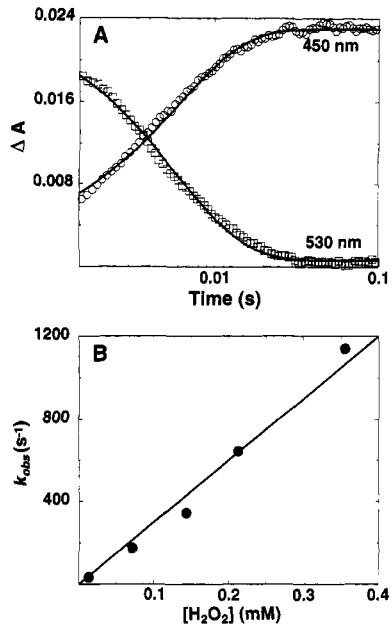

FIGURE 11: Stopped-flow analysis of the reaction of H_2O_2 with Npx EH_2. (A) EH_2 (17.5 μM) was mixed with 70 μM H_2O_2 at pH 7.0, 5 °C, using the Applied Photophysics instrument. The course of the reaction was monitored at 450 nm (○) and at 530 nm (□). (B) Pseudo-first-order rate constants for the oxidation of EH_2 at several concentrations of H_2O_2 are plotted *versus* [H_2O_2]. All data were collected at pH 7.0, 5 °C.

DISCUSSION

On the basis of our earlier analysis of the steady-state kinetics of the recombinant NADH peroxidase (Parsonage et al., 1993), we proposed a limiting type of ternary complex mechanism using the Type II(i) scheme originally described by Dalziel (1957) as a guide. However, as discussed by Dalziel, this general case cannot be distinguished from an alternative with eight calculable rate constants [Type II(ii,a)], and the latter is preferred. The combined steady-state and rapid-reaction data presented in this report are consistent with the modified kinetic mechanism given:

$$EH_2 + NADH \underset{k_2}{\overset{k_1}{\rightleftharpoons}} EH_2\cdot NADH^*$$

$$EH_2\cdot NADH^* + H_2O_2 \underset{k_4}{\overset{k_3}{\rightleftharpoons}} E\cdot NADH + H_2O$$

$$E\cdot NADH + H^+ \underset{k_3'}{\overset{k_4'}{\rightleftharpoons}} EH_2\cdot NAD^+ + H_2O$$

$$EH_2\cdot NAD^+ \underset{k_1'}{\overset{k_2'}{\rightleftharpoons}} EH_2 + NAD^+$$

The distinction between the two schemes is the absence of a formal EH_2·NADH·H_2O_2 central complex and the two rate constants describing its interconversion with E·NADH. EH_2 is generated in an initial priming step, and the EH_2·NADH* complex indicated above corresponds to the catalytically competent species identified in this work. Using the kinetic coefficients defined by Dalziel (1957), Tables 2 and 3 give both the observed and calculated parameters determined from the steady-state and stopped-flow data presented in this

Table 2: Kinetic Coefficients for the NADH Peroxidase Reaction and Their Experimental Values

kinetic coefficient	kinetic equivalent[a]	values from steady-state data[b]
ϕ_0	$1/k_2' + 1/k_4'$	4.29×10^{-2} s (1.18×10^{-1} s)
ϕ_{NADH}	$1/k_1$	1.29×10^{-7} M s (3.17×10^{-7} M s)
$\phi_{H_2O_2}$	$1/k_3$	6.05×10^{-7} M s
$\phi_{NADH \cdot H_2O_2}$	$k_2/(k_1k_3)$	0[c]

[a] Adapted from the general Type II(ii,a) case described by Dalziel (1957), with the specific condition that $k_4 = 0$ (see Discussion). [b] Values determined from the kinetic parameters at pH 7.0 as given in Table 1. Values in parentheses represent ϕ_0(AcPyADH) and $\phi_{AcPyADH}$ constants determined similarly. [c] See Discussion.

Table 3: Comparison of Steady-State and Stopped-Flow Results for NADH Peroxidase

kinetic parameter	steady-state value	stopped-flow value
K_m(NADH)	3.0 μM	6.1 μM
$K_m(H_2O_2)$	14.1 μM	7.7 μM
k_{cat}	23.3 s^{-1}	23.0 s^{-1}
ϕ_0	4.29×10^{-2} s	4.34×10^{-2} s
ϕ_{NADH}	1.29×10^{-7} M s	2.63×10^{-7} M s
$\phi_{H_2O_2}$	6.05×10^{-7} M s	3.33×10^{-7} M s
k_1	7.75×10^6 M^{-1} s^{-1} [a]	4.1×10^6 M^{-1} s^{-1}
k_2	0	ND[b]
k_3	1.65×10^6 M^{-1} s^{-1}	3.0×10^6 M^{-1} s^{-1} [c]
k_4		0[c]
k_4'		25.4 s^{-1}
k_3'		0[d]
k_2'		250 s^{-1}
k_1'	ND	

[a] Steady-state values for specific rate constants were calculated from the corresponding kinetic coefficients, using the kinetic equivalents given in Table 2. Similarly, stopped-flow values for the steady-state kinetic parameters were calculated from the experimentally-determined rate constants. [b] ND, not determined. [c] Determined from the $[H_2O_2]$ dependency for the oxidation of $EH_2 \rightarrow E$. [d] NAD^+ cannot oxidize $EH_2 \rightarrow E$.

report. The kinetics of the priming reaction ($E \rightarrow EH_2$) have been analyzed in the presence of stoichiometric NADH, and the rate of conversion of EH_2·NADH* to the static EH_2·NADH species has also been determined. The latter is not catalytically competent, and this distinction between these two substrate complexes represents another major feature of the revised scheme. Although the direct reaction of EH_2·NADH* with H_2O_2 has not been measured, we have investigated the kinetics of H_2O_2 reduction by EH_2, and the rate constants describing this reaction are given in Table 3. Based on the irreversible second-order kinetics of this reaction, the existence of a frank EH_2·NADH·H_2O_2 "ternary complex" in turnover is considered even less likely, lending further support to the revised scheme. The E·NADH species observed in both enzyme-monitored turnover experiments and in the reduction of $E \rightarrow EH_2$ is formally analogous to the EXY central complex described in the generalized Dalziel mechanism (Dalziel, 1957). Since only H_2O has been formed as a product at this stage, the peroxidase kinetic scheme should be equivalent to the Type II(ii,a) mechanism.

The general form of the corresponding initial rate equation is:

$$\frac{e}{v_0} = \phi_0 + \frac{\phi_1}{[NADH]} + \frac{\phi_2}{[H_2O_2]} + \frac{\phi_{12}}{[NADH][H_2O_2]}$$

Previous steady-state analyses of both the recombinant *E. faecalis* peroxidase (Parsonage et al., 1993) and the enzyme from *E. hirae* (Stoll & Blanchard, 1988) are consistent, however, with a classical ping-pong mechanism, indicating that $\phi_{12} = 0$. From Dalziel, $k_2 = \phi_{12}/(\phi_1\phi_2)$ for any Type II mechanism; therefore, $k_2 = 0$ for the peroxidase, and the binding of NADH to EH_2 is effectively irreversible. The reaction of EH_2 with H_2O_2 is also irreversible; since we consider this reaction to be representative of the H_2O_2 oxidation of EH_2·NADH*, k_4 is very likely equal to zero as well. Also, since we have demonstrated that NAD^+ cannot reoxidize $EH_2 \rightarrow E$, $k_3' = 0$. For this specific case, the kinetic coefficients are:

$$\phi_0 = 1/k_2' + 1/k_4'$$

$$\phi_1 = 1/k_1$$

$$\phi_2 = 1/k_3$$

The steady-state parameters k_{cat}, K_m(NADH), and $K_m(H_2O_2)$ are defined in terms of these coefficients (Dalziel, 1957). As shown in Table 3 for the steady-state and stopped-flow data collected at pH 7.0, 5 °C, there is excellent agreement between the observed and calculated values for k_{cat}. This supports the conclusion that the hydride transfer from bound substrate in the conversion of E·NADH $\rightarrow$ EH_2 (k_4') is largely rate-limiting in turnover and that NAD^+ release from EH_2 (k_2'), although still partially rate-limiting, is relatively rapid. The requirement for H^+ in enzyme reduction, coupled with the near-equivalence of k_{cat} and k_4', is also consistent with the acidic pH optimum indicated in the k_{cat} profile. The pH-dependent decrease in k_4' (25.4 $s^{-1} \rightarrow$ 5.6 s^{-1}) over the range 7.0−8.5 accounts almost quantitatively for the accompanying change in k_{cat}.

Steady-state values for ϕ_{NADH} at pH 7.0 and 8.5 correspond to $k_1 = 7.75 \times 10^6$ M^{-1} s^{-1} and 4.88×10^6 M^{-1} s^{-1}, respectively, at 5 °C. Given the very rapid association observed for EH_2 and NADH in the stopped-flow, relative to the 1.5-ms dead time measured for our instrument, we were limited in our ability to accurately determine the second-order rate constant for formation of EH_2·NADH*. In the presence of 4- and 5-fold excesses of NADH, k_{obs} values of 573 s^{-1} and 848 s^{-1} were obtained for this process at EH_2 concentrations of 23 and 88 μM, respectively. Since $k_2 = 0$, the corresponding values for k_1 at pH 7.0, 5 °C, are 6.2×10^6 and 1.9×10^6 M^{-1} s^{-1}, and the average is given in Table 3. In order to provide further experimental support for this aspect of the peroxidase mechanism, we carried out a detailed analysis of AcPyADH as a substrate at pH 7.0, 5 °C. From the steady-state data given in Table 1, $\phi_{AcPyADH} = 3.17 \times 10^{-7}$ M s, and the corresponding value for k_1 (AcPyADH) is 3.15×10^6 M^{-1} s^{-1}. With a 3-fold excess of AcPyADH, $k_{obs} = 281$ s^{-1} was determined for the formation of EH_2·AcPyADH* at an EH_2 concentration of 42.2 μM. The observed second-order rate constant of 2.2×10^6 M^{-1} s^{-1} agrees well with the calculated value of 3.15×10^6 M^{-1} s^{-1}.

Since $K_m(H_2O_2) = \phi_{H_2O_2}/\phi_0$, the nearly 13-fold decrease in this parameter over the pH range 7.0−8.5 can be quantitatively accounted for by the observed change in k_{cat}, provided there is an accompanying increase in k_3. Although the pH profile for $k_{cat}/K_m(H_2O_2)$ was determined at 25 °C, it does provide evidence for a limiting ionization with a pK_a

of ~7.5 which promotes the reaction of the reduced enzyme with H_2O_2. This would provide the required increase in $k_{cat}/K_m(H_2O_2)$, which represents a lower limit for the value of k_3, at pH 8.5. At pH 7.0, 5 °C, the reaction of $EH_2 + H_2O_2 \rightarrow E + H_2O$ shows irreversible second-order kinetics, giving $k_3 = 3.0 \times 10^6$ M^{-1} s^{-1}. As shown in Table 3, this value compares very favorably with that calculated (1.65×10^6 M^{-1} s^{-1}) from the steady-state parameter $\phi_{H_2O_2}$. Since we are taking the EH_2 reaction as representative of that for EH_2·NADH*, intrinsic differences for these enzyme species in their H_2O_2 reactivities will be reflected in the comparison of calculated and observed values for k_3. We have also shown that the peroxide reaction with the static EH_2·NADH complex is slower than turnover.

Of the eight calculable rate constants involved in the kinetic mechanism for the peroxidase, the combined steady-state and stopped-flow analyses presented in this report leave only k_1', the second-order rate constant for NAD^+ binding to EH_2, undetermined. Stoll and Blanchard (1988) were unable to demonstrate product inhibition by NAD^+ with NADH as substrate at pH 7.5, 25 °C, even at [NAD^+] >5 mM and [NADH] as low as 3.3 μM, with the *E. hirae* peroxidase. A $K_i(NAD^+)$ value of 0.54 mM was, however, determined with the poor reducing substrate NADPH. The observed lack of inhibition in the presence of NADH is consistent with mutually exclusive binding of either NAD^+ or NADH to EH_2, but with a relatively rapid off-rate for NAD^+ ($k_2' = 250$ s^{-1} at pH 7.0, 5 °C, for the *E. faecalis* peroxidase; this work) and very rapid, effectively irreversible binding of NADH ($k_1 = 4.1 \times 10^6$ M^{-1} s^{-1} at pH 7.0, 5 °C; this work). Since NAD^+ titration of EH_2 did not give rise to any significant spectral changes, direct stopped-flow measurement of k_1' was not possible.

The pK_a of ~7.5 observed in the $k_{cat}/K_m(H_2O_2)$ profile is consistent with the proposal (Poole & Claiborne, 1989a) that peroxide reduction involves nucleophilic attack by the Cys42-thiolate of EH_2 (as EH_2·NADH*), but we have shown that the Cys42-S^- species is fully ionized at pH 5.4 (Poole & Claiborne, 1986). The low pK_a of Cys42-SH, in particular, is compatible with the acidic pH optimum in the k_{cat} profile; enzyme reduction is optimized without affecting the requirement for Cys42-thiolate in the peroxide reaction. The crystal structure of the peroxidase E(Cys42-SO_3H)·NADH complex (Stehle et al., 1993) originally led to the proposal of an ion pair between a protonated His10 and the Cys42-thiolate in EH_2·NADH, but this suggestion has been brought into question by recent studies of the wild-type and C42S mutant peroxidase active-site structures (Mande et al., 1995). In the C42S mutant His10 is hydrogen-bonded to the charged guanidinium moiety of Arg303, and the presence of a similar Arg303−His10 interaction in the wild-type peroxidase makes it very likely that His10 remains unprotonated throughout the catalytic cycle. It is therefore also unlikely that His10 accounts for either of the limiting pK_a values observed in the k_{cat} and $k_{cat}/K_m(H_2O_2)$ profiles of the peroxidase. Since flavin-mediated reduction of Cys42-SOH by bound NADH (E·NADH → EH_2) is largely rate-limiting over the pH range studied, it is possible that the pK_a of 6.9 ± 0.2 in the k_{cat} profile represents ionization of Cys42-SOH to the Cys42-sulfenate (Cys42-SO^-; Poole & Claiborne, 1989a). Tripolt et al. (1993) have determined the sulfenic acid pK_a for the unusually stable 4,6-dimethoxy-1,3,5-triazine-2-sulfenic acid to be 5.86. Quantitative data on the ionization of alkanesulfenic acids are not available, however (Claiborne et al., 1993), and it is difficult to interpret the pK_a data for these aromatic sulfenic acids relative to Cys42-SOH of the peroxidase.

Recently, Rietveld et al. (1994) have reported the kinetic analysis of both wild-type and H439A mutant *E. coli* glutathione reductases; direct observation of FAD reduction by NADPH is seen only in the mutant because of the very slow intramolecular reoxidation of $FADH_2$ effected by His439 replacement. With wild-type GR, limiting rate constants of 310−330 s^{-1}, 245−270 s^{-1}, and 110 s^{-1} were attributed to (1) hydride transfer from bound NADPH to FAD, (2) displacement of $NADP^+$ by NADPH, and (3) reduction of the disulfide by $FADH_2$. Although the present scheme for peroxidase reduction does bear some similarities, neither diode-array nor fixed-wavelength stopped-flow analyses allow identification of a discrete $FADH_2$ intermediate, and the primary deuterium isotope effect is measured on the conversion of E·NADH → EH_2(FAD, Cys42-SH). We have recently shown (Parsonage & Claiborne, 1995) that NADH reduction of the peroxidase C42S mutant rapidly yields E($FADH_2$)·NAD^+ ($k_{obs} = 290$ s^{-1} at 0.2 mM NADH, 5 °C), and the NAD^+ off-rate of 134 s^{-1} can be compared to the k_2' value of 250 s^{-1} from this work. The FAD/$FADH_2$ redox potential for the C42S peroxidase is 93 mV more positive than that for EH_2, supporting the conclusion that the Cys42-thiolate strongly influences the redox properties of the FAD. In contrast, the FAD redox potential in the GR C47S mutant (replacing the charge-transfer Cys) is very low (−449 mV at pH 8.4; Rietveld et al., 1994), and the stable E·NADPH complex which results on anaerobic addition of substrate has spectral properties very similar to the wild-type peroxidase E·NADH intermediate described in this report. Rietveld et al. (1994) have suggested that an additional influence on the FAD/$FADH_2$ redox potential involves the differential binding of pyridine nucleotide to the respective forms of the C47S mutant, and a very similar effect must explain the absence of flavin reduction in the stable peroxidase EH_2·NADH complex.

In summary, the mechanism presented in this report provides the necessary framework for future investigations combining enzyme kinetics, site-directed mutagenesis, and X-ray crystallographic approaches, with the overall goal of developing a structure-based understanding of the redox chemistry catalyzed by this unique flavoprotein peroxidase.

ACKNOWLEDGMENT

We would like to thank Dr. David P. Ballou, Department of Biological Chemistry, University of Michigan, for providing access to the diode-array stopped-flow spectrophotometer in his laboratory and for his guidance and helpful discussions during the course of this work.

REFERENCES

Claiborne, A., Ross, R. P., & Parsonage, D. (1992) *Trends Biochem. Sci. 17*, 183−186.

Claiborne, A., Miller, H., Parsonage, D., & Ross, R. P. (1993) *FASEB J. 7*, 1483−1490.

Claiborne, A., Ross, R. P., Ward, D., Parsonage, D., & Crane, E. J., III (1994) in *Flavins and Flavoproteins 1993* (Yagi, K., Ed.) pp 587−596, de Gruyter, New York.

Dalziel, K. (1957) *Acta Chem. Scand. 11*, 1706−1723.

Frieden, C. (1993) *Trends Biochem. Sci. 18*, 58−60.

Gibson, Q. H., Swoboda, B. E. P., & Massey, V. (1964) *J. Biol. Chem. 239*, 3927−3934.
Gutfreund, H. (1972) *Enzymes: Physical Principles*, pp 190−194, John Wiley & Sons, New York.
Leatherbarrow, R. (1987) *Enzfitter*, Biosoft, Hills Road, Cambridge, U.K.
Loach, P. A. (1976) in *Handbook of Biochemistry and Molecular Biology* (Fasman, G. D., Ed.) 3rd ed., Vol. 1, pp 122−130, CRC Press, Boca Raton, FL.
Mande, S. S., Parsonage, D., Claiborne, A., & Hol, W. G. J. (1995) *Biochemistry 34*, 6985−6992.
Miller, H., Poole, L. B., & Claiborne, A. (1990) *J. Biol. Chem. 265*, 9857−9863.
Miller, H., Mande, S. S., Parsonage, D., Sarfaty, S. H., Hol, W. G. J., & Claiborne, A. (1995) *Biochemistry 34*, 5180−5190.
Miller, S. M., Ballou, D. P., Massey, V., Williams, C. H., Jr., & Walsh, C. T. (1986) *J. Biol. Chem. 261*, 8081−8084.
Orr, G. A., & Blanchard, J. S. (1984) *Anal. Biochem. 142*, 232−234.
Ottolina, G., Riva, S., Carrea, G., Danieli, B., & Buckmann, A. F. (1989) *Biochim. Biophys. Acta 998*, 173−178.
Parsonage, D., & Claiborne, A. (1995) *Biochemistry 34*, 435−441.
Parsonage, D., Miller, H., Ross, R. P., & Claiborne, A. (1993) *J. Biol. Chem. 268*, 3161−3167.
P-L Biochemicals Circular No. OR-18 (1977) P-L Biochemicals, Milwaukee, WI.
Pollegioni, L., Fukui, K., & Massey, V. (1994) *J. Biol. Chem. 269*, 31666−31673.
Poole, L. B., & Claiborne, A. (1986) *J. Biol. Chem. 261*, 14525−14533.
Poole, L. B., & Claiborne, A. (1989a) *J. Biol. Chem. 264*, 12330−12338.
Poole, L. B., & Claiborne, A. (1989b) *J. Biol. Chem. 264*, 12322−12329.
Rietveld, P., Arscott, L. D., Berry, A., Scrutton, N. S., Deonarain, M. P., Perham, R. N., & Williams, C. H., Jr. (1994) *Biochemistry 33*, 13888−13895.
Ross, R. P., & Claiborne, A. (1991) *J. Mol. Biol. 221*, 857−871.
Ross, R. P., & Claiborne, A. (1992) *J. Mol. Biol. 227*, 658−671.
Stehle, T., Ahmed, S. A., Claiborne, A., & Schulz, G. E. (1991) *J. Mol. Biol. 221*, 1325−1344.
Stehle, T., Claiborne, A., & Schulz, G. E. (1993) *Eur. J. Biochem. 211*, 221−226.
Stoll, V. S., & Blanchard, J. S. (1988) *Arch. Biochem. Biophys. 260*, 752−762.
Tripolt, R., Belaj, F., & Nachbaur, E. (1993) *Z. Naturforsch. 48b*, 1212−1222.
Veine, D. M., Arscott, L. D., & Williams, C. H., Jr. (1994) in *Flavins and Flavoproteins 1993* (Yagi, K., Ed.) pp 497−500, de Gruyter, New York.
Walsh, C. T., Distefano, M. D., Moore, M. J., Shewchuk, L. M., & Verdine, G. L. (1988) *FASEB J. 2*, 124−130.
Williams, C. H., Jr. (1992) in *Chemistry and Biochemistry of Flavoenzymes* (Müller, F., Ed.) Vol. III, pp 121−211, CRC Press, Boca Raton, FL.

BI951082K